MEDDOCS Open Access Publisher

Nanoscience and Nanotechnology: Open Access

Open Access | Research Article

Interaction of Chlorophyll with Artificial Colorants in Restricted Nanoscopic Environment: Key Insights on the Toxicity from Electronic Spectroscopy

Amrita Banerjee[1,2]; Dipanjan Mukherjee[3]; Md. Nur Hasan[3]; Subhadipta Mukhopadhyay[1]; Debjani Karmakar[4,5]; Ranjan Das[6]; Arpita Chattopadhyay[7]*; Samir Kumar Pal[3]*

[1]Department of Physics, Jadavpur University, 188, Raja S.C. Mallick Rd, Kolkata 700032, India.

[2]Technical Research Centre, S. N. Bose National Centre for Basic Sciences, Block JD, Sector III, Salt Lake, Kolkata, West Bengal 700106, India.

[3]Department of Chemical and Biological Sciences, S. N. Bose National Centre for Basic Sciences, Block JD, Sector 3, Salt Lake, Kolkata-700106, India.

[4]Department of Physics and Astronomy, Uppsala University Box 516, Uppsala SE-75120, Sweden.

[5]Technical Physics Division, Bhabha Atomic Research Centre, Mumbai, 400085, India.

[6]Department of Chemistry, West Bengal State University, Barasat, North 24 PGS, Kolkata 700126

[7]Department of Basic Science and Humanities, Techno International New Town Block - DG 1/1, Action Area 1New Town, Rajarhat, Kolkata- 700156, India.

Corresponding Author(s): Arpita Chattopadhyay[1] & Samir Kumar Pal[2]

[1]Department of Chemical and Biological Sciences, S. N. Bose National Centre for Basic Sciences, Block JD, Sector 3, Salt Lake, Kolkata-700106, India.

[2]Department of Basic Science and Humanities, Techno International New Town Block - DG 1/1, Action Area 1 New Town, Rajarhat, Kolkata -700156, India.

Email: skpal@bose.res.in & arpita.chattopadhyay@tict.edu.in

Received: Apr 19, 2023

Accepted: June 27, 2023

Published Online: June 30, 2023

Journal: Nanoscience and Nanotechnology: Open Access

Publisher: MedDocs Publishers LLC

Online edition: http://meddocsonline.org/

Abstract

Chlorophyll is a vital component of vegetables and fruits which are essential dietary requirements to maintain a healthy lifestyle and many of them have anticancer properties. However, they are frequently adulterated by unscrupulous business practices with toxic illegal dyes for making their appearance fresh and vibrant. On the other hand, chlorophyll may interact with harmful dyes and heavy metals by virtue of its strong tendency of complex formation by the porphyrin ring when root of plants starts consumption from dye contaminated soils with industry or agricultural effluents. Our experimental findings vividly reveal the interaction of chlorophyll with three commonly used illegal dyes, namely copper sulfate, malachite green, and sudan red in a restricted nanoscopic environment of an anionic micelle (SDS). The hypsochromic shift of around 10 nm in the chlorophyll absorbance band supports the copper metal binding and fluorescence quenching and Time Correlated Single Photon Counting (TCSPC) investigations confirmed the nature of dynamic quenching of the chlorophyll emission. The increase of the absorbance peak in the presence of the dye malachite green indicates that dimers of the dye are likely to develop. The absorption peak at the blue end is most pronounced at the maximum concentration of the

Cite this article: Pal SK, Chattopadhyay A, Banerjee A, Mukherjee D, Nur Hasan MD, et al. Interaction of Chlorophyll with Artificial Colorants in Restricted Nanoscopic Environment: Key Insights on the Toxicity from Electronic Spectroscopy. Nanosci Nanotechnol Open Access. 2023; 2(1): 1012.

malachite green dye, at the expense of a weakening of the absorption band at 470 nm. The static quenching mechanism is supported by further considerable fluorescence quenching of chlorophyll after inner filter effect correction and picosecond time resolved analysis with malachite green addition. The likelihood of Forster Resonance Energy Transfer (FRET) between chlorophyll-SDS and sudan red dye due to their overlapping emission and absorption spectral signatures was investigated and an energy transfer efficiency of roughly 15% was obtained between the doner and acceptor, establishing a modest interaction. The hazardous effects of the dyes on human are also thoroughly investigated using predictive computational biology technique.

Keywords: Chlorophyll; Interaction with dyes; Spectroscopic studies; Adulteration of vegetables; Sensor; Chemical-protein interaction.

Introduction

The protective role of fruits and vegetables consumption against chronic lifestyle diseases, like cancer and cardiovascular disease has been established quite a few decades back in several studies [1-4]. The potential defensive mechanism of fruits and vegetables are strongly associated with their constituents, namely, antioxidants, vitamins, pigments like chlorophylls, flavonoids etc [5]. However, in recent decades, adulteration of food items, especially in vegetables, fruits, spices, and beverages has become a major concern to public health. According to the U.S. Food and Drug Administration (FDA), the main incentive behind the irresponsible adulteration is financial gain, known as Economically Motivated Adulteration (EMA). In EMA, the actual components and ingredients of foods are either deliberately substituted by some cheaper products, or its real appearance gets more attractive and fresher by external modifications [6]. Before reaching to the consumer, an untrusted entity can cause adulteration of food at any of the stages of growth, processing, transportation, and supply of food by multiple entities in the delivery chain [7].

Human health is food-sensitive, and thus acute or chronic exposure to adulterated products can have a long-term adverse health impact. Adulterated food consumption is directly associated to major health risks such as liver, vision, skin, and stomach disorders [8]. To make the appearance of fruits and vegetables more fresh, dangerous industrial dyes, like sudan dyes I-IV, metanil yellow, malachite green, copper sulphate, rhodamine B are often used, which can create severe damage to public health in the long run [9]. Additionally, there are evidence that the dye additives cause genotoxicity, carcinogenicity and hypersensitivity [10]. Among common inedible and harmful chemical dyes used to make vegetables look fresh and vibrant [9], for the current work, three widely-used dyes were chosen viz., copper sulphate, malachite green, and sudan red to study their interactions with chlorophyll.

Copper sulphate, a toxic chemical known for its ability to affect liver [11] is widely used in food industry for its re-greening properties on vegetables. $CuSO_4$ is toxic for humans if an amount of >1 gm is ingested [12], with symptoms ranging from mild nausea to severe gastrointestinal infections along with other disorders [13]. On the other hand, copper is a common non-biodegradable heavy metal which can accumulate in soils for a long period of time due to anthropogenic activity such as the use of chemical fertilizers, adulterant dyes, sewage, industrial and smelting wastes [14], and can be taken up by the root system of plants via diffusion, endocytosis or metal transporters [15-26]. Although Cu is an important micronutrient that constitute plastocyanin and cytochrome oxidase essential for photosynthesis and respiration which have a crucial function in plant carbon assimilation and ATP generation excessive levels of Cu intake in plants can lead to oxidative stress that causes severe damage to membranes and macromolecules, as well as having a severe negative impact on many metabolic pathways [27-29]. Cu-stressed plants exhibit a variety of visible symptoms, including chlorosis, stunted development, ion leakage and reduced growth of roots [30]. Thus, elaborate study of the interaction of copper and its compounds with chlorophyll is essential to explore the potential risks for plants and animals.

To enhance the freshness and appearance of green vegetables like gourds, peas and beans [31], malachite green is also used, which acts as a tumour promoter, by inducing the formation of reactive oxygen species [32]. Malachite Green (MG) a triphenylmethane dye, is a multiple use compound that is mainly used in textile industries and partly used in aquaculture in fungicides and ectoparasiticides [33,34]. It also possesses carcinogenic and genotoxic properties which pose a potential risk to humans and therefore, this dye has been banned in Europe, the USA and several countries [33]. Furthermore, the MG dye in water may be accumulated in plant tissue and inhibit growth of the plants [35,36].

Use of the sudan dyes was also reported to pose serious threat, as its excessive use may lead to liver cancer like severe diseases [37]. Animal studies have already predicted the neurotoxic and hepatotoxic nature of metanil yellow [38].

The detailed interaction of Chlorophyll with the harmful dyes, viz, copper sulphate, malachite green and sudan red III are studied in the current study using absorption and emission spectroscopy along with Time-Correlated Single Photon Counting (TCSPC) technique. The dyes may directly interact with the chlorophyll of fruits and vegetables, either by unethical fraudulent practices of adulteration to keep them fresh, or through intake of dye contaminated soils with industrial or agricultural effluents through the root of plants. In plants, chlorophylls are not freely available, they are encapsulated in granum. To create the similar restrictive nanoscopic environment in our study, Sodium Dodecyl Sulfate (SDS) micelle was used, which, like granum, confine the chlorophyll. To establish the harmful effects of these dangerous dyes at the molecular level, computational biology technique was also employed in this study.

Materials and Methods

Chemicals

Analytical grade Sodium Dodecyl Sulphate (SDS), Malachite Green (MG), Copper Sulphate pentahydrate ($CuSO_4$,$5H_2O$), Sudan Red (SR), Dimethyl Sulfoxide (DMSO) were purchased from Sigma Aldrich, California and used with no further purification. Vegetables used in this study were procured from local supermarket of Kolkata, India.

Sample preparation

20 mM, 3 mM, 5 mM and 4 mM stock solutions of SDS, MG and $CuSO_4$ in DI water (Milli-Q) and SR in DMSO were prepared. The solutions were further diluted according to the experimental study. All the measurements were performed at room tem-

perature.

Extraction of Chlorophyll

Fresh Neem (Azadirachta Indica) leaves (100 gm) were cut into small pieces (approximately 1 cm×1 cm). The pieces were ground in a mortar (5 mins), 95% Iso-Propyl Alcohol (IPA) (50 mL) was added and the mixture was homogenized for 3-5 mins or until a light green solution was obtained (Figure 1). The solution was kept overnight and after extraction the solution was filtered through what man filter papers and the filtrate was collected.

Photophysical Studies

Steady state and time-resolved fluorescence spectroscopy: Absorption spectra of chlorophyll were measured with Shimadzu spectrophotometer (model UV-2600, Shimadzu, Japan) in the 200-800 nm wavelength range. The room temperature steady-state emission spectra were recorded using a Fluorolog Model LFI-3751 (Horiba-Jobin Yvon, Edison, NJ, USA) spectrofluorometer equipped with a microchannel plate photomultiplier tube (MCP-PMT, Hamamatsu, Japan). All fluorescence spectra were corrected to account for wavelength variations in source intensity, photomultiplier response, and monochromator throughput. All the picosecond resolved fluorescence transients were measured by using commercially available TCSPC setup with Microchannel plate-based photomultiplier tubes (MCP-PMT) from Edinburgh instrument, U.K. (instrument response function (IRF) of ~75 ps) using a 630 nm excitation laser source. All the fluorescence transients have been measured in magic angle 550. In our study, Chlorophyll (chl) and sudan red act as the donor and acceptor respectively. The non-emissive behaviour of the dyes eliminates the possibility of the interference of SR in chl fluorescence transients in SDS micelle. Details of the time resolved fluorescence setup have been discussed in our previous reports [39,40]. Fourier Transform Infrared Spectroscopy (FTIR) on the liquid samples were performed using a JASCO FTIR-6300 spectrometer instrument (Oklahoma City, OK, USA).

Fitting of picosecond resolved fluorescence transients

The observed fluorescence transients were fitted by using a nonlinear least-squares fitting procedure to a function

$$(X(t) = \int_0^t E(t')R(t-t')dt') \quad (1)$$

(E(t)) with a sum of exponentials (1) with pre-exponential factors (B_i),

$$(R(t) = A + \sum_{i=1}^{N} B_i e^{-t/\tau_i} \quad (2)$$

With characteristic lifetimes (τ_i) and a background (A). Relative concentration in a multiexponential decay is expressed as,

$$c_n = \frac{B_n}{\sum_{i=1}^{N} B_n} \times 100 \quad (3)$$

The amplitude-weighted average lifetime of a multiexponential decay is expressed as,

$$\tau_{av} = \sum_{i=1}^{N} c_i \tau_i \quad (4)$$

$$\sum_{i=1}^{N} c_i = 1 \quad (5)$$

The quality of the transients fitting has been justified by observing reduced chi-square which is none other than the ratio of residual and weighted residual. In the transients fitting, the value of χ^2 lies in between 1.0 to 1.2.

Forster resonance energy transfer (FRET) studies

In order to estimate the Forster resonance energy transfer (FRET) efficiency from the donor to the acceptor and to determine the donor-acceptor pairs we have followed the methodology described in Lakowicz [41]. The critical donor-acceptor distance (R_0) where the energy transfer efficiency is 50% was calculated using the formula below:

$$R_0 = 0.211 \times [\kappa^2 n^{-4} Q_D J(\lambda)]^{\frac{1}{6}} \quad (6)$$

The refractive index (n) is considered to be 1.43. k^2 is the orientational factor describing the relative orientation of the transition dipoles of donor and acceptor respectively in space. The orientational factor, k^2 is mathematically related to the cosine of the orientational angle as follows:

$$\kappa^2 = (cos\theta_T - 3cos\theta_D - cos\theta_A)$$

where θ_T is the angle in between the transition dipole of the donor and acceptor respectively; θ_D and θ_A are the angle in between donor and acceptor dipole and the vector that joins the donor and acceptor dipole respectively. The donor and the acceptor are assumed to adopt all possible orientation during the energy transfer process for which the value of κ^2 is taken to be 0.667. Because sixth root of the orientational factor is considered the maximum error introduced in determining the donor acceptor distance is not more than 30%. Q_D is the quantum yield of the donor in the absence of acceptor is measured to be 0.01 by considering quinine sulphate as a reference of Quantum Yield (QY) determination.

$J(\lambda)$ is the overlap integral which signifies the degree of spectral overlap between the donor emission and the acceptor absorption and is expressed as:

$$J(\lambda) = \frac{\int_0^\infty F_D(\lambda)\varepsilon_A(\lambda)\lambda^4 d\lambda}{\int_0^\infty F_D(\lambda)d\lambda} \quad (7)$$

The D–A pair distance (r_{DA}) can be calculated after getting the value of R_0 from the following equation.

$$r_{DA}^6 r^6 = \frac{[R_0^6(1-E)]}{E} \quad (8)$$

E is the energy transfer efficiency calculated from the lifetimes of the donor in absence and in presence of the acceptor (τ_D and τ_{DA}).

$$E = 1 - \frac{\tau_{DA}}{\tau_D} \quad (9)$$

τ_D is the average lifetime of the donor and τ_{DA} is the average lifetime of the donor in presence of acceptor, obtained from the fitted parameters of the fluorescence transients.

Computational Methods

The first principles density functional theoretical calculations have been performed to investigate the electronic structure of Chl and Chl-Cu (II) using Vienna ab initio simulation package (VASP). The spin-polarised plane-wave methods were employed within Generalized Gradient Approximation and Perdew-Burke-Ernzerhof exchange correlation functional and projector augmented wave pseudopotentials. The ionic relaxations were achieved with a conjugate gradient algorithm till

the Hellmann-Feynmann force are lower than 0.001 eV/Å on each ion. The k-meshes are prepared by using Monkhorst-Pack grid, plane-wave cut-off energy was chosen to be 500 eV and convergence was set to 10^{-6} eV. The ionically relaxed structures were used to calculate the electronic density of states by using Gaussian smearing.

Separate computational tools were used to study compound-protein interaction. To predict Chemical-Protein (CP) Interaction Networks of the quercetin, the STITCH tool (http://stitch.embl.de/) was used, whose database stores around 10 million protein and 5 million chemical information [42,43]. In this database, the predictive value of a particular chemical-protein interaction can be controlled by the confidence score and for the present study the value was kept at 0.4.

Results and Discussion

FTIR spectra of the extract from leaves in the spectral range of 4000-0 cm^{-1} revealed the presence of chlorophyll as depicted in Figure 1a. As observed from the functional groups of the chlorophyll dye extracted from *Azadirachta Indica* in Figure 1a, the vibrations of $C\text{-}H_3$ and $C\text{-}H_2$ bonds are obtained at 2916.2 cm^{-1} and 2844.7 cm^{-1}[44, 45] respectively. Moreover, absorption band occurring at around 1721 cm^{-1} [44, 46] is attributed due to the C=O bond and the C-O vibration at 1045 cm^{-1} [44] is prominent also. The C-N vibration of porphyrins at 145 cm^{-1} are also observed [47]. The signature of the OH bond stretching can be witnessed at 3330cm^{-1} [46,48]. The Mg-N peak is visible at 301cm^{-1} [49]. Finally, the absorption band at 1644 cm^{-1} is due to the presence of the C=C bond [50].

Interactions of extracted Chlorophyll (chl) from leaves with different dyes commonly used to adulterate fruits and vegetables are investigated in a restricted nanoscopic environment of SDS micelles analogous to granum where chlorophylls are naturally restricted. The isosbestic point at 629 nm for chlorophyll a and b is considered for excitation in this study [51]. The absorbance and emission of the extracted chlorophyll along with its physical appearance are shown in Figure 1b. The absorbance maxima at 664 nm and 611nm and emission 672 nm are exactly matching with that of pure chlorophyll [46] confirming the proper extraction of chlorophyll.

Spectroscopic investigations of the nature of interactions of Chl-Cu(II) systems within the micellar cavity

The main absorption bands in the Chl-Cu(II) (Figure 2a) spectra are mainly generated due to electronic transitions between π and π* orbitals of the macrocycle of the Metallochlorophylls complex, quite similar to that of metalloporphyrins. The effect of metal binding on the spectral properties of the chlorophyll has been systematically investigated by Gouterman [52,53], which is later backed by the theoretical calculations of Orzel et.al. And Sundholm's [54,55]. In our study, Chl is attached to the negatively charged surface of the SDS micelle. During gradual addition of the $CuSO_4$ at increasing concentrations to the Chl-SDS complex, significant changes in absorption spectra have been observed, among them the most significant are [1], hypsochromic shift at around 660 to 670 nm of the QY band from its original position; [2]. Significant hypsochromisms in the UV-Vis absorption of the low intensity bands at around 500 nm; [3]. Hypsochromisms in the highest intensity bands around 400 nm. Substitution of the Mg^{2+} metal ion into the tetrapyrrolic cavity by other ions depends on the competitive binding affinity which brings a strong impact mainly on the electronic state of the macrocycle and consequent absorption spectra as well. Hypsochromic shift of the Q_Y band clearly indicates the formation of a complex with the added metal ion. The features of the Q_Y bands at several concentrations of $CuSO_4$ are quite dramatic and do not follow the regular pattern. It follows an initial decrease followed by further reconstruction of the absorption band, but the reconstructed band is not identical in terms of absorption intensity as well as wavelength as that of starting one by which it discards the possibility of the reversible interaction. Reduction of the absorption intensity around the 400 nm central band as well as hypochromicity around 500 nm are the clear signature of the formation of an intermediate complex where both the metals ions (Mg^{2+} and Cu^{2+}) are held by the macrocyclic ring. Irreversibility of the 650 nm absorption band at highest $CuSO_4$ concentration discards the complete substitution of the Mg^{2+} by the Cu^{2+}.

The corresponding fluorescence spectra of the chlorophyll display no considerable shift of the peak position with increasing concentration of $CuSO_4$, however the intensity decreases gradually (Figure 2b). This quenching of fluorescence intensity might be due to the formation of SDS-Chl-Cu^{2+} ion pair, which progressively associate to form an aggregated type of structure. The same nature of fluorescence quenching has also been observed with increasing concentration of Cu^{2+} in absence of Chl alone in water. To interpret the nature of quenching, we have monitored the fluorescence lifetime since both $\frac{I_0}{I}$ or $\frac{\tau_0}{\tau}$ directly related to the quenching ability of a quencher. At 50 µM concentration of $CuSO_4$, the excited state lifetime of the Chl in SDS reduces from 1.13 ns to 0.347 ns and the change of (τ_0/τ) matches well with that of intensity (I_0/I) confirming the dynamic nature of the quenching (Figure 2c). In contrary, Chl in water in presence of Cu^{2+} shows no changes in excited state lifetime which is the signature of the static nature of the quencher where the ground state population of Chl has been perturbed by the quenchers (Figure 2c inset).

To investigate the electronic property and charge transfer mechanism in the hybrid system, we have performed first principles density functional theory calculations. Figure 3a and b show the ionically relaxed structure of Chl and Chl-Cu (II) using a -point centred single k-point calculation. The Chl-Cu (II) has replaced the Mg ion of Chl by Cu ion (56). The formation energy of the Chl-Cu (II) system is -0.15 eV/atom which indicates the feasibility of formation and structural stability of Chl-Cu (II). Figure 3c shows the atom-projected partial density of states (APDOS) of pure Chl and Figure 3d shows the APDOS of Chl-Cu (II). Pristine Chl is seen to have an energy-gap of ~1.4 eV between Valence Band Maxima (VBM) and Conduction Band Minima (CBM). The CBM has mostly constituted by N-2*p* and C-2*p* orbital. There is a significant reduction of energy bandgap for Chl-Cu (II) due to presence of some additional ligand levels states (Figure 2d) of constituting N-2*p* and C-2*p* orbitals. There is a structural reconstruction around the metal ion associated with the replacement of Mg with Cu because of the difference in the radii of Mg^{2+} (0.65 Å) and Cu^{2+} (0.73 Å) as well as the additional spin-polarization incorporated within the system due to the substitution of the non-magnetic atom Mg with magnetic atom Cu. This reconstruction of the structure leads to the modification of the ligand levels and are thereby responsible due to the modification of band gap [57]. The theoretically predicted results support the experimental findings of modification of the optical properties due to the change of the electronic interaction.

Spectroscopic investigations of the nature of interactions of Chl-MG systems within the micellar cavity

Absorption spectra of the Chl-SDS upon interaction with MG at various concentrations are shown in Figure 2d. As observed from the figure, Chl in SDS produces an absorption band around 400 nm and 600 nm, which progressively increases in terms of intensity upon addition of MG at various concentrations. Intensifying the peak at position 600 nm in the spectrum indicates the formation of an adduct of MG with Chl-surfactant complex. Shukla et. al. (58) earlier reported such interaction between a cationic dye, crystal violet and Chl, resulting in the formation of a new band in the blue region of the absorption spectrum. Such an interaction might also lead to the formation of dimers of the dye. The absorption peak at the blue end is strengthened most at highest MG concentration, at the expense of the weakening of the 470 nm absorption band. Isosbestic point at 500 nm reveals coexistence of two different species in the medium.

The fluorescence spectrum of Chl in SDS strongly corroborates with the spectral nature of Chl in water. The observed decrease in fluorescence intensity of Chl in the presence of MG can (Figure 2e) arise either due to the various quenching mechanisms or even through non-molecular mechanisms where self-absorption of the fluorophores may screen the emissive light. To find out the possibility we have corrected the emission spectra by considering the absorption of the absorbing species (equation 10) (59):

$$F_{Corr} = F_{Obs} \times \exp((A_{ex} + A_{em})/2) \qquad (10)$$

where F_{Cor} and F_{Obs} are the corrected and observed fluorescence intensities, respectively; A_{ex} and A_{em} are the absorbance of the system at excitation and emission wavelength, respectively. After correction we observe MG induces significant quenching of the Chl which further discards the possibility of inner filter effect of fluorescence quenching. To understand the quenching mechanism, we have further monitored excited state lifetime of Chl-SDS complex at various MG concentrations since alternatively the quenching process can be expressed in terms of $\frac{\tau_0}{\tau}$. The constant value of τ_0/τ confirms the static nature of the quenching (Figure 2f and Table I).

Table 1: Time-resolved decay parameters of chlorophyll in SDS in absence and in presence of copper sulphate, malachite green and sudan red dyes at different concentrations. Reactant (R) stands for 2 ml 20 mM SDS +300 uM chlorophyll.

System	τ1 (ns)/%	τ2 (ns)/%	τ3 (ns)/%	τ_{avg} (ns)	χ^2
Reactant (R)	0.327 (53%)	1.40 (20%)	5.67 (27%)	2.19	1.17
R+20 uM Sudan Red	0.192 (51%)	0.930 (21%)	5.82 (28%)	1.94	1.01
R+40 uM Sudan Red	0.156 (52%)	0.879 (17%)	5.89 (31%)	2.03	1.02
Reactant(R)	0.141 (60%)	0.763 (24%)	5.50 (16%)	1.13	1.04
R+5 uM $CuSO_4$	0.140 (70%)	0.877 (17%)	3.29 (13%)	0.678	0.99
R+20 uM $CuSO_4$	0.037 (59%)	0.572 (20%)	1.55 (21%)	0.463	0.99
R+40 uM $CuSO_4$	0.030 (58%)	0.426 (20%)	1.13 (21%)	0.349	0.89
Reactant(R)	0.223 (59%)	1.00 (21%)	5.56 (20%)	1.46	1
R+20 uM MG	0.149 (58%)	0.817 (24%)	5.70 (18%)	1.25	1.05
R+40 uM MG	0.060 (66%)	0.674 (22%)	5.68 (12%)	0.856	1.09

Spectroscopic investigations of the nature of interactions of Chl with a foreign dye Sudan Red within the micellar cavity

In our study, we have made an attempt to capture the interaction of sudan red as a food adulterant [60] with Chl. Since sudan red has an absorption tail around the emission tail of Chl (Figure 2g), it is assumed that there is a possibility of FRET (Forster Resonance Energy Transfer) between Chl-SDS and Sudan red. After spectral correction in steady state emission spectra, energy transfer efficiency has been obtained at ~ 15% (Figure 2h). Energy transfer efficiency has been calculated as $E = 1 - \frac{F_{DA}}{F_D}$; F_{DA} and F_D are the fluorescence intensity of the donor in presence and in absence of acceptor. To further verify the energy transfer efficiency, we have monitored the excited state lifetime in absence and in presence of sudan red. By using τ_D and $\tau_{DA,}$ the calculated energy transfer efficiency obtained as ~ 18% which clearly supports the observed fluorescence quenching in steady state (Figure 2i). It is evident that by monitoring FRET efficiency, one can monitor the presence of other foreign molecules like sudan red as an adulterant specially in vegetables.

Table 2: Chemical-protein interaction and activity of copper sulphate, sudan red and malachite green.

Name of the chemical	Name of the interacting protein	Activity
Copper sulphate	HSPA4 /heat shock 70kDa protein 4	In vivo and in vitro studies have shown that heat shock proteins (HSPs), detected in both the prokaryotic and eukaryotic cells, enhances its level after environmental stresses, infection, normal physiological processes, gene transfer, thus plays a crucial role in the survival of organisms.
	SLC31A2(CTR2) / solute carrier family 31 (copper transporters), member 2;	CTR2 plays an important role in mammalian Cu homeostasis and is involved in low-affinity copper uptake (Potential)
	ATP7B / ATPase, Cu++ transporting, beta polypeptide;	It is involved in the export of copper out of the cells, such as the efflux of hepatic copper into the bile. Almost 60 diseases have now been reported in connection with specific mutations of ATP7B in patients with Wilson's disease, a genetic disorder of copper metabolism.
	TRPV1 / transient receptor potential cation channel, subfamily V, member 1;	It is involved in detection of noxious chemical and thermal stimuli. TRPV1 may provide connection between the process of inflammation, cancer and immunity, which can be useful to cultivate new treatment pathways.
	AQP3 / aquaporin 3 (Gill blood group);	Water channel promotes glycerol permeability and water transport across cell membranes and acts as a glycerol transporter in skin and plays an important role in regulating stratum corneum and epidermal glycerol content and involved in skin hydration, wound healing, and tumorigenesis.
	TYR / tyrosinase	This is a copper-containing oxidase that functions in the formation of pigments such as melanin and other polyphenolic compounds and have the potential applications like design of inhibitors of undesirable fruit browning in vegetables or of colour skin modulators in animals.

	JUN / jun proto-oncogene	Although it is not identified as a cancer-specific chromosomal translocation, but its dominant negative mutants weaken the growth of various tumour cells.
	AKT1/ v-akt murine thymoma viral oncogene homolog 1	AKT1 is one of 3 closely related serine/threonine- protein kinases which regulate many processes including metabolism, cancer proliferation, cell survival, growth and angiogenesis.
	FOXO1 / forkhead box O1 and FOXO4 / forkhead box O4	Transcription factor that is the main target of insulin signalling and regulates metabolic homeostasis in response to oxidative stress. It is also involved in processes like apoptosis, cell cycle arrest, stress resistance, cellular differentiation and development, and tumor suppression
Sudan Red	CCNA1 / cyclin A1	Loss of cyclin A1 may lead to disruption of male sterility due to cell arrest in the late diplotene stage of the meiotic cell cycle
	CCDC90A / coiled-coil domain containing 90A	Key regulator of mitochondrial calcium uniporter (MCU) required for calcium entry into mitochondrion. Plays a direct role in uniporter-mediated calcium uptake, possibly via a direct interaction with MCU
	UQCRFS1 / ubiquinol-cytochrome c reductase, Rieske iron-sulfur polypeptide 1	Component of the ubiquinol-cytochrome c reductase complex (complex III or cytochrome b-c1 complex), which is a respiratory chain that generates an electrochemical potential coupled to ATP synthesis. Isolated complex III (CIII) deficiency symptoms range from isolated myopathy to severe multi-systemic disorders, even early death and disability.
	CELA1 / chymotrypsin-like elastase family, member 1	Acts upon elastin
	CDC123 / cell division cycle 123 homolog (S. cerevisiae)	It has a crucial role in protein biosynthesis by supplying methionylated initiator tRNA to the ribosomal translation initiation complex.
	HHEX / hematopoietically expressed homeobox	Its enforced expression may induces T-cell leukaemia.
	CCDC90B / coiled-coil domain containing 90B	It is important agent for fusion, signalling, and scaffolding.
	CCNA2 / cyclin A2	It is essential for the control of the cell cycle at the G1/S (start) and the G2/M (mitosis) transitions. It is also a potential target for prevention of tamoxifen resistance.
Malachite green	BCHE / butyrylcholinesterase	Contributes to the inactivation of the neurotransmitter acetylcholine. Can degrade neurotoxic organophosphate esters. It is a perfect indicator of pesticide poisoning and nerve agent exposure.
	KCNH2 / potassium voltage-gated channel, subfamily H (eag-related), member 2	Its dysfunction may lead to intrauterine fetal death, sudden infant death syndrome, cardiac arrhythmia, and sudden cardiac death
	KCNA3 / potassium voltage-gated channel, shaker-related subfamily, member 3	Mediates the voltage-dependent potassium ion permeability of excitable membranes. It also regulates neurotransmitter release, insulin secretion, neuronal excitability, immune response, apoptosis, and cell proliferation.
	GSTP1 / glutathione S-transferase pi 1	This enzyme can detoxify the cell from endogenous and exogenous toxic compounds by using glutathione (GSH).

Computational studies to predict the harmful effects of dyes on human health

Chlorophyll, the primary pigment responsible for the green colour in vegetables and plants, with their limited bioavailability, reported to have oxidative stress regulating capacity, hence has a preventative role in cancer initiation and progression [61]. Studies [62,63] have shown that plant pigments, including chlorophyll are able to bind mutagens, also inhibit the absorption, and stop mutagens to interact with DNA. However, when the vegetables are adulterated with harmful industrial chemical and dyes like copper sulphate, malachite green and sudan red, the dyes may create serious health hazards. Table 2 provides a comprehensive analysis regarding the chemical-protein interaction for the current study, as depicted in Figure 4.

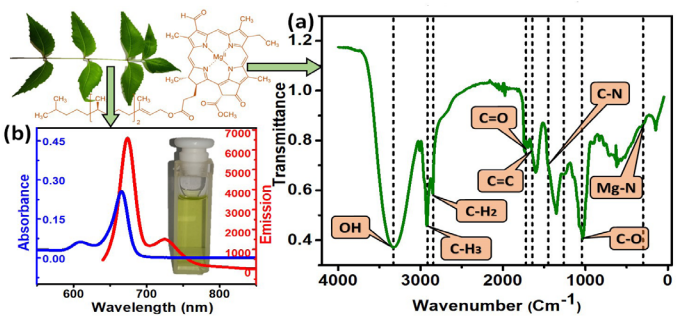

Figure 1: Extraction and characterization of chlorophyll from leaves **(a)** FTIR spectrum of the extracted chlorophyll in the range 0-4000cm^{-1} **(b)** Absorbance (blue) and emission (red) spectra of the extracted chlorophyll. The recorded emission is for excitation at the isosbestic point of chlorophyll a and b (629nm). Inset shows the physical appearance of the extracted chlorophyll after filtration.

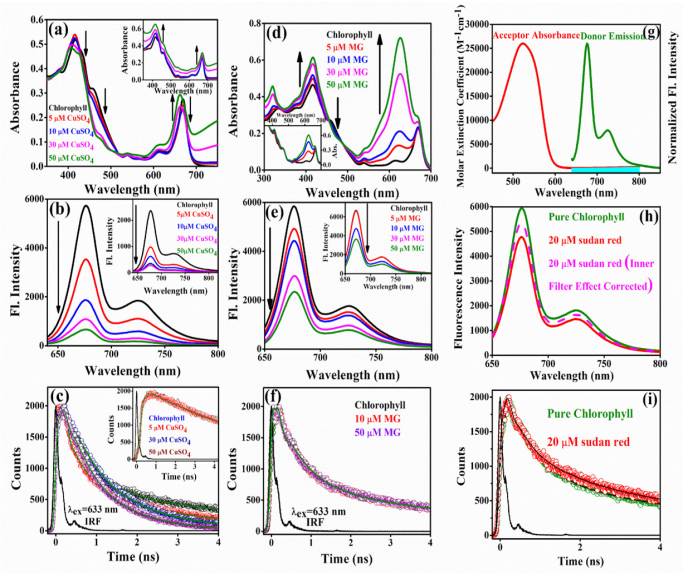

Figure 2: Interaction of chlorophyll with $CuSO_4$ in terms of **(a)** Absorbance **(b)** Emission and **(c)** TCSPC in SDS micelles for 5-50uM concentrations of $CuSO_4$ (insets show absorbance, emission and TCSPC in water respectively). Interaction of chlorophyll with malachite green in terms of **(d)** Absorbance **(e)** Emission and **(f)** TCSPC in SDS micelles for 5-50 uM concentrations of MG (insets show absorbance, emission and TCSPC in water respectively). **(g)** Spectral overlap of chl fluorescence (green) and SR absorbance (red) when both are incorporated in SDS micelle. **(h)** Forster Resonance Energy Transfer (FRET) process is of chl ligand to SR within the SDS micelle is evident from the quenching of the steady-state fluorescence intensity after inner filter effect correction **(i)** Picosecond-resolved fluorescence transients of the chl ligand as donor in SDS micelle in absence and in presence of SR as an acceptor.

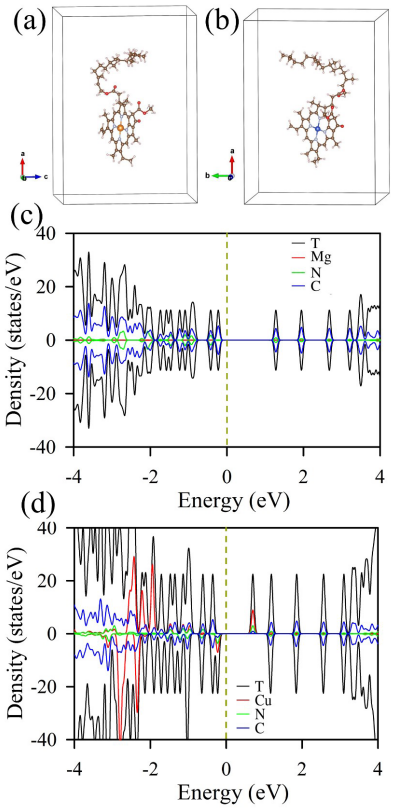

Figure 3: Ionic relaxed structure of **(a)** chlorophyll and **(b)** chlorophyll-Cu (II). The partial density of states (PDOS) **(c)** chlorophyll and **(d)** chlorophyll-Cu (II).

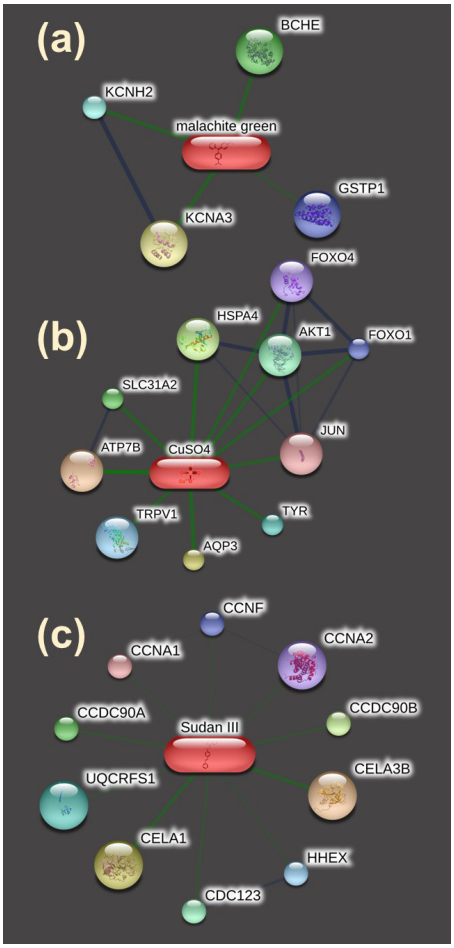

Figure 4: Chemical protein interaction of **(a)** Malachite green **(b)** Copper sulphate and **(c)** Sudan Red using Computational Biology.

Conclusion

The present work has demonstrated, the detailed mechanism of interactions of chlorophyll with some harmful dyes. The dyes can be interlinked directly with chlorophyll of fruits and vegetables either by unscrupulous business practices of adulteration for making items fresh and vibrant or by consumption through root of plants from dye contaminated soils with industry or agricultural effluents. The experimental findings reveal the interaction of chlorophyll with three commonly used illegal dyes, namely copper sulphate, malachite green, and sudan red in a restricted nanoscopic environment of SDS micelles. For copper sulphate, the hypsochromic shift of 10nm in the absorbance band of chlorophyll confirms the metal binding and fluorescence quenching as well as TCSPC studies revealed the nature of dynamic quenching. The intensification of absorbance peak in presence of the dye malachite green is indicative of probable formation of dimers of the dye. The absorption peak at the blue end is strengthened most at the highest concentration of the MG dye, at the expense of weakening of the 470 nm absorption band. Further significant fluorescence quenching of chlorophyll after inner filter effect correction and picosecond time resolved analysis with addition of malachite green indicate the static quenching mechanism. The possibility of FRET between the chlorophyll-SDS and sudan red dye due to their overlapped emission and absorbance spectral signatures was explored and around 15% energy transfer efficiency was obtained between the doner and acceptor establishing a mild interaction. The hazardous effects of the dyes on human are also thoroughly investigated using predictive computational biology technique.

Acknowledgement

SKP wants to thank Indian National Academy of Engineering (INAE) for the Abdul Kalam Technology Innovation National Fellowship, INAE/121/AKF. We acknowledge the Thematic Unit of Excellence on Computational Material Science, S N. Bose Centre, for providing the CRAY computational facility.

Conflict of interest: The authors declare no conflict of interest.

References

1. Steinmertz K, Potter J. Vegetables, fruit and cancer epidemiology. Cancer Causes Cont. 1991; 2: 325-357.
2. Howe GR, Hirohata T, Hislop TG, Iscovich JM, Yuan J-M, et al. Dietary factors and risk of breast cancer: combined analysis of 12 case-control studies. JNCI: Journal of the National Cancer Institute. 1990; 82: 561-569.
3. Joshipura KJ, Hu FB, Manson JE, Stampfer MJ, Rimm EB, et al. The effect of fruit and vegetable intake on risk for coronary heart disease. Annals of internal medicine. 2001; 134: 1106-1114.
4. Rao BN. Bioactive phytochemicals in Indian foods and their potential in health promotion and disease prevention. Asia Pacific Journal of clinical nutrition. 2003; 12.
5. Laura A, Alvarez-Parrilla E, González-Aguilar GA. Fruit and vegetable phytochemicals: chemistry, nutritional value and stability: John Wiley & Sons. 2009.
6. EMILIA DMER. Blockchain-based traceability of the food supply chain: consumer perception and a case study.
7. Schell LM, Gallo MV, Cook K. What's NOT to eat-food adulteration in the context of human biology. American Journal of Human Biology. 2012; 24: 139-148.
8. Bansal S, Singh A, Mangal M, Mangal AK, Kumar S. Food adulteration: Sources, health risks, and detection methods. Critical reviews in food science and nutrition. 2017; 57: 1174-1189.
9. Oplatowska-Stachowiak M, Elliott CT. Food colors: Existing and emerging food safety concerns. Critical reviews in food science and nutrition. 2017; 57: 524-548.
10. Kobylewski S, Jacobson MF. Toxicology of food dyes. International journal of occupational and environmental health. 2012; 18: 220-246.
11. Scotter MJ, Castle L, Roberts D. Method development and HPLC analysis of retail foods and beverages for copper chlorophyll (E141 [i]) and chlorophyllin (E141 [ii]) food colouring materials. Food additives and contaminants. 2005; 22: 1163-1175.
12. Gamakaranage CS, Rodrigo C, Weerasinghe S, Gnanathasan A, Puvanaraj V, Fernando H. Complications and management of acute copper sulphate poisoning; a case discussion. Journal of occupational medicine and toxicology. 2011; 6: 1-5.
13. Shomaji S, Masna NVR, Ariando D, Deb Paul S, Horace-Herron K, Forte D, et al. Detecting dye-contaminated vegetables using low-field NMR relaxometry. Foods. 2021; 10: 2232.
14. Aydinalp C, Marinova S. The effects of heavy metals on seed germination and plant growth on alfalfa plant Medicago sativa. Bulgarian Journal of Agricultural Science. 2009; 154: 347-50.
15. Öztürk MA. Plants and Pollutants in Developped and Developing Countries: International Symposium Held in Izmir, Turkey, 22-28 August, 1988; Botany Department, Science Faculty, Ege University, Bornova: Ege University Press; 1989.
16. Ali I, Jain CK. Advances in arsenic speciation techniques. International Journal of Environmental Analytical Chemistry. 2004; 84: 947-964.
17. Krzesłowska M. The cell wall in plant cell response to trace metals: polysaccharide remodeling and its role in defense strategy. Acta physiologiae plantarum. 2011; 33: 35-51.
18. Ali I, Gupta VK, Khan TA, Asim M. Removal of arsenate from aqueous solution by electro-coagulation method using Al-Fe electrodes. Int J Electrochem Sci. 2012; 7:1898-1907.
19. Ali I, ALOthman ZA, Sanagi MM. Green synthesis of iron nano-impregnated adsorbent for fast removal of fluoride from water. Journal of Molecular Liquids. 2015; 211: 457-465.
20. Suhail M, Ali I. Advanced spiral periodic classification of the elements. Chem Int. 2017; 3: 220-224.
21. Ali I, Alharbi OM, Alothman ZA, Badjah AY, Alwarthan A. Artificial neural network modelling of amido black dye sorption on iron composite nano material: kinetics and thermodynamics studies. Journal of Molecular Liquids. 2018; 250: 1-8.
22. Sabir M, Waraich EA, Hakeem KR, Ozturk M, Ahmad HR, et al. Phytoremediation: mechanisms and adaptations. Soil remediation and plants: prospects and challenges. 2014; 85: 85-105.
23. Dehghani MH, Sanaei D, Ali I, Bhatnagar A. Removal of chromium (VI) from aqueous solution using treated waste newspaper as a low-cost adsorbent: kinetic modeling and isotherm studies. Journal of molecular liquids. 2016; 215: 671-679.
24. Alharbi OM, Khattab RA, Ali I. Health and environmental effects of persistent organic pollutants. Journal of Molecular Liquids. 2018; 263: 442-453.
25. Basheer AA. New generation nano-adsorbents for the removal of emerging contaminants in water. Journal of Molecular Liquids. 2018; 261: 583-593.
26. Burakova EA, Dyachkova TP, Rukhov AV, Tugolukov EN, Galunin EV, et al. Novel and economic method of carbon nanotubes synthesis on a nickel magnesium oxide catalyst using microwave radiation. Journal of Molecular Liquids. 2018; 253: 340-346.
27. Singh H, Kumar D, Soni V. Copper and mercury induced oxidative stresses and antioxidant responses of Spirodela polyrhiza (L.) Schleid. Biochemistry and Biophysics Reports. 2020; 23: 100781.
28. Raj S, Singh H, Trivedi R, Soni V. Biogenic synthesis of AgNPs employing Terminalia arjuna leaf extract and its efficacy towards catalytic degradation of organic dyes. Scientific reports. 2020; 10: 9616.
29. Yadav S. Heavy metals toxicity in plants: an overview on the role of glutathione and phytochelatins in heavy metal stress tolerance of plants. South African journal of botany. 2010; 76: 167-179.
30. Bouazizi H, Jouili H, Geitmann A, El Ferjani E. Copper toxicity in expanding leaves of Phaseolus vulgaris L. antioxidant enzyme response and nutrient element uptake. Ecotoxicology and environmental safety. 2010; 73: 1304-1308.
31. Ashok V, Agrawal N, Durgbanshi A, Esteve-Romero J, Bose D. Determination of adulteration of malachite green in green pea and some prepared foodstuffs by micellar liquid chromatography. Journal of AOAC International. 2014; 97: 1387-1392.
32. Panandiker A, Fernandes C, Rao K. The cytotoxic properties of malachite green are associated with the increased demethylase, aryl hydrocarbon hydroxylase and lipid peroxidation in primary cultures of Syrian hamster embryo cells. Cancer letters. 1992; 67: 93-101.

33. Srivastava S, Sinha R, Roy D. Toxicological effects of malachite green. Aquatic toxicology. 2004; 66: 319-29.

34. Fu X-Y, Zhao W, Xiong A-S, Tian Y-S, Zhu B, et al. Phytoremediation of triphenylmethane dyes by overexpressing a Citrobacter sp. triphenylmethane reductase in transgenic Arabidopsis. Applied Microbiology and Biotechnology. 2013; 97: 1799-1806.

35. Herklotz PA, Gurung P, Vanden Heuvel B, Kinney CA. Uptake of human pharmaceuticals by plants grown under hydroponic conditions. Chemosphere. 2010; 78: 1416-1421.

36. Szczygłowska M, Piekarska A, Konieczka P, Namieśnik J. Use of Brassica Plants in the Phytoremediation and Biofumigation Processes. International Journal of Molecular Sciences. 2011; 12: 7760-7771.

37. Fonovich TM. Sudan dyes: are they dangerous for human health? Drug and Chemical Toxicology. 2013; 36: 343-352.

38. Nagaraja TN, Desiraju T. Effects of chronic consumption of metanil yellow by developing and adult rats on brain regional levels of noradrenaline, dopamine and serotonin, on acetylcholine esterase activity and on operant conditioning. Food and Chemical Toxicology. 1993; 31: 41-44.

39. Choudhury S, Mondal PK, Sharma V, Mitra S, Sakai VG, et al. Direct observation of coupling between structural fluctuation and ultrafast hydration dynamics of fluorescent probes in anionic micelles. The Journal of Physical Chemistry B. 2015; 119: 10849-10857.

40. Mukherjee D, Singh P, Rakshit T, Puthiya-Purayil TP, Vemula PK, et al. Deciphering the response of asymmetry in the hydrophobic chains of novel cationic lipids towards biological function. Physical Chemistry Chemical Physics. 2020; 22: 1738-1746.

41. Lakowicz J. Principles of Fluorescence Spectroscopy; 2 edn, chap. 6. Kluwer Academic/Plenum Publisher. New York, Boston, Dordrecht, London, Moscow; 1999.

42. Szklarczyk D, Santos A, Von Mering C, Jensen LJ, Bork P, et al. STITCH 5: Augmenting protein-chemical interaction networks with tissue and affinity data. Nucleic acids research. 2016; 44: D380-D384.

43. Kuhn M, Szklarczyk D, Pletscher-Frankild S, Blicher TH, Von Mering C, et al. STITCH 4: integration of protein–chemical interactions with user data. Nucleic acids research. 2014; 42: D401-D407.

44. Chang H, Kao M-J, Chen T-L, Chen C-H, Cho K-C, et al. Characterization of natural dye extracted from wormwood and purple cabbage for dye-sensitized solar cells. International Journal of Photoenergy. 2013; 2013.

45. Merck. Ir Spectrum Table by Frequency Range. 2023; 25.

46. Ahmed JK, Amer ZJA, Al-Bahate MJM. Effect of chlorophyll and anthocyanin on the secondary bonds of Poly Vinyl Chloride (PVC). International Journal of Materials Science and Applications. 2015; 4: 21-9.

47. Suica-Bunghez Ir, Sorescu Aa, Doncea Sm, Constantin M, Raut I, et al. Phytochemical, antioxidant and antimicrobial characterization of Hedera helix L. extract. Journal of Plant Development. 2020; 27.

48. Hemmalakshmi S, Priyanga S, Devaki K. Fourier Transform Infra-Red Spectroscopy Analysis of Erythrina variegata L. Journal of Pharmaceutical Sciences and Research. 2017; 9: 2062-2067.

49. Mojumdar S, Melnik M, Jona E. Thermal decomposition and IR spectra of Mg (II) compounds with caffeine. CHEMICAL PAPERS-SLOVAK ACADEMY OF SCIENCES. 1999; 53: 309-314.

50. Darmokoesoemo H, Fidyayanti AR, Setyawati H, Kusuma HS. Synthesis of complex compounds Ni (II)-chlorophyll as Dye Sensitizer in Dye Sensitizer Solar Cell (DSSC). Korean Chemical Engineering Research. 2017; 55: 19-26.

51. Guidi L, Tattini M, Landi M. How does chloroplast protect chlorophyll against excessive light. Chlorophyll. 2017; 21: 21-36.

52. Gouterman M. Optical spectra and electronic structure of porphyrins and related rings. The porphyrins. 1978; 3.

53. Gouterman M, Wagni re GH, Snyder LC. Spectra of porphyrins. Journal of Molecular Spectroscopy. 1963; 11: 108-27.

54. Orzel L, Szmyd B, Rutkowska-Zbik D, Fiedor L, van Eldik R, et al. Fine tuning of copper (II)-chlorophyll interactions in organic media. Metalation versus oxidation of the macrocycle. Dalton Transactions. 2015; 44: 6012-6022.

55. Sundholm D. Comparison of the electronic excitation spectra of chlorophyll a and pheophytin a calculated at density functional theory level. Chemical Physics Letters. 2000; 317: 545-552.

56. Küpper H, Setlík I, Spiller M, Kupper FC, Prasil O. Heavy metal-induced inhibition of photosynthesis: targets of in vivo heavy metal chlorophyll formation1. Journal of Phycology. 2002; 38: 429-441.

57. Bechaieb R, Fredj AB, Akacha AB, Gérard H. Interactions of copper (II) and zinc (II) with chlorophyll: insights from density functional theory studies. New Journal of Chemistry. 2016; 40: 4543-4549.

58. Shukla D, Pandey FP, Kumari P, Basu N, Tiwari MK, et al. Label-Free Fluorometric Detection of Adulterant Malachite Green Using Carbon Dots Derived from the Medicinal Plant Source Ocimum tenuiflorum. ChemistrySelect. 2019; 4: 4839-4847.

59. Mukherjee D, Singh P, Singh S, Roy DS, Singha S, et al. Host assisted molecular recognition by human serum albumin: Study of molecular recognition controlled protein/drug mimic binding in a microfluidic channel. International Journal of Biological Macromolecules. 2021; 176: 137-144.

60. Trentanni Hansen GJ, Almonacid J, Albertengo L, Rodriguez MS, Di Anibal C, et al. NIR-based Sudan I to IV and Para-Red food adulterants screening. Food Additives & Contaminants: Part A. 2019; 36:1163-1172.

61. Hayes M, Ferruzzi MG. Update on the bioavailability and chemopreventative mechanisms of dietary chlorophyll derivatives. Nutrition Research. 2020; 81: 19-37.

62. Simonich MT, Egner PA, Roebuck BD, Orner GA, Jubert C, et al. Natural chlorophyll inhibits aflatoxin B 1-induced multi-organ carcinogenesis in the rat. Carcinogenesis. 2007; 28: 1294-1302.

63. Jubert C, Mata J, Bench G, Dashwood R, Pereira C, Tracewell W, et al. Effects of chlorophyll and chlorophyllin on low-dose aflatoxin B1 pharmacokinetics in human volunteers. Cancer prevention research. 2009; 2: 1015-1022.